Numerical study a flow around a heated finite cylinder and mounted vertically on a flat plate

Hamza GOUIDMI[1, 2], Razik BENDERRADJI[1,3], Abdelhadi BEGHIDJA[1]
[1]Laboratory of Renewable Energies and Sustainable Development (LERDD), Frères Mentouri University, Constantine1-Algeria
[2]Mohamed El-Bachir El-Ibrahimi University, Bordj Bou Arréridj- Algeria
[3]Mohamed Boudiaf University, M'Sila- Algeria
gouidmi@yahoo.fr

Abstract: - Flow around a finite end cylinder mounted vertically on a flat plate and thermally heated is simulated numerically by the Large-Scale Simulation (LES) approach. The flow is in subcritical regime circulate with a velocity U_∞=0.54m/s corresponding a Reynolds number $Re_D=2.2x10^4$. The boundary condition of Neumann is imposed on the surface of the cylinder, which is reflected by a density of the heat flux is ϕ= 600W/m^2, for an aspect ratio H/D=5.This simulation induces a complex structure of the flow behind the cylinder, in particular the appearance of vortices and recirculation zones ahead and behind it. The results obtained give a clear comparison with those found experimentally and numerically of Guillermo Palau-Salvador et al. [2], that were carried out its work in the case of adiabatic flow.

Key-Words: - Heated Cylinder, Vortex Structures, Mixed Convection.

Abbreviations:
TFC: Horseshoe vortex.
VKV: Von Kàrmàn vortex
KHV: Whirlwind of Kelvin Helmholtz
BV: wake whirlpools
TM: Marginal vortices
Re: Reynolds Number
Nu: Nusselt Number
Pr : Prandtl Number

1 Introduction

These phenomena are classical but they exist and encountered in industrial applications, especially combined phenomena between thermal and dynamic transfer, such as cylindrical buildings, piles or cooling towers placed in the atmospheric boundary layer where it interacts with the wind, cooling fins of computer processors, rods in various technical equipment such as fuel or central rods in nuclear power plants and open channels. The flows around the thermally heated free-end cylinders add other nascent complex secondary vortices above and behind them, because they are three-dimensional nature and very unstable character. However, globally, several parameters affecting these vortex phenomena, we quote: The Reynolds number, the aspect ratio defined by H/D (H is the height of the cylinder and D the diameter) and the shape of the cylinder...etc. It has for example the effect of aspect ratio on the overall structure of the nascent vortices in Fig.1 driven by Kawamura et al. [1]. Many experimental and numerical scientific works have treated these phenomena, such as the works of [1], [2], [3], [4], [5]. The technological development of computer hardware has improved the calculations of complex problems and compared them with experience.

Flow around a circular cylinder at a free end thermally heated and vertically mounted on a flat plate for an aspect ratio H/D=5 is simulated numerically by the LES approach, using the Fluent 6.3 calculation code. However, the study is carried out with a heat flux imposed on the surface of the cylinder is 600W/m^2. This work is based on experimental studies of [2] and [3] by adding the thermal study we heating the cylinder. We will

analyze and treat it after the obtained results, such as the average and fluctuating fields as well as the average Nusselt number.

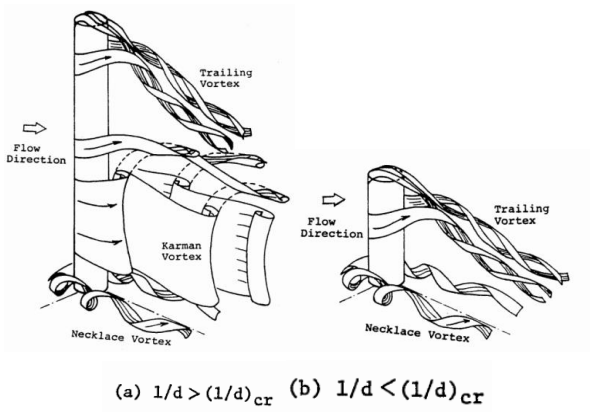

Fig.1: Vortices structures for two different aspect ratios, Boizumault et al. [1].

2 Configuration and numerical model

2.1 Test configuration

The geometry used in numerical simulations is shown in Fig. 2. It is a three-dimensional cylinder of circular section mounted on a horizontal wall. The cylinder has a diameter D= 0.04 m and a height H= 0.2 m. Its aspect ratio AR=H/D= 5. The length of the computation domain is L=1.52 m, its height is 0.4 m and its depth is 0.56 m. The center of the cylinder is placed as a reference direct orthogonal, is located 0.32m downstream of the entrance face. Then, the blocking factor (S/S_o), defined by the ratio between the surfaces of the cylinder projected on the input surface is about 3.5%. The boundary condition imposed on the surface of the cylinder is verified by the Neumann condition, which is signified by a heat flux density equal 600W/m^2.

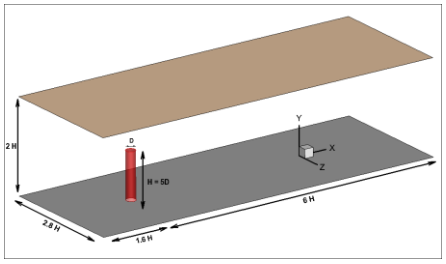

Fig. 2: Geometry and dimensions of the configuration.

The fluid used is water, passing through the cylinder with a uniform velocity U_∞=0.54m/s giving a Reynolds number based on the diameter of the cylinder of the order of Re = 2.2x10^4. The numerical simulations were carried out on a 3D control space with implicit temporal discretization of the second order. The dimensioning and the inlet flow parameters are shown in Table 1.

Table 1 : Dimensions and input parameters

D (m)	H (m)	U_∞ (m/s)	AR	S/S_o	Re
0.04	0.2	.54	H/D=5	0.035	2.2.10^4

2.2 Numerical model

2.2.1 Description

The flow is considered incompressible in physical properties constant. The calculation scheme chosen makes it possible to solve the averaged filtered Navier-Stokes equations (spatial averaging) implicitly to find the temperature, the velocity and the pressure, such as conservation equations of mass, momentum and energy.

2.2.2 Large Eddy Simulation; LES

In the assumptions of viscous incompressible flow, the continuity, momentum and energy equations filtered take the following form:

$$\frac{\partial \bar{u}_i}{\partial x_i} = 0 \tag{1}$$

$$\frac{\partial \bar{u}_i}{\partial t} + \frac{\partial (\bar{u}_i \bar{u}_j)}{\partial x_j} = -\frac{1}{\rho}\frac{\partial \bar{p}}{\partial x_i} + \nu \frac{\partial^2 \bar{u}_i}{\partial x_i \partial x_j} - \frac{\partial \tau_{ij}}{\partial x_j} \tag{2}$$

$$\frac{\partial \bar{T}}{\partial t} + \frac{\partial (\bar{u}_j \bar{T})}{\partial x_j} = -\frac{\nu}{Pr}\frac{\partial^2 \bar{T}}{\partial x_j \partial x_j} - \frac{\partial \phi_j}{\partial x_j} \tag{3}$$

Where ρ is the density of the fluid, ν is the kinematic viscosity, $\bar{T}$ is the filtered temperature, $\bar{u}_i$is the filtered velocity, $\bar{P}$ is the filtered pressure. ϕ_j and $\tau_{ij}$are the heat flux and stress tensor in the subgrid scale, respectively, defended by the following relations:

$$\phi_j = \overline{u_j T} - \bar{u}_j \bar{T} \tag{4}$$

$$\tau_{ij} = \overline{u_i u_j} - \bar{u}_i \bar{u}_j \tag{5}$$

The standard Smagorinsky model is used in this work to modeled the stresses and heat flux in the subgrid scale (SGS).

The origin of this model is based on the assumption of equilibrium between production and dissipation for small scales. In this model, the stresses and heat fluxes on the subgrid scale are calculated with the dynamic approach of Germano et al. [6] as modified by Lilly et al. [7], which models the anisotropic part of the term SGS, which is written as follows:

$$\tau_{ij}^{*} = \tau_{ij} - \frac{1}{3}\tau_{kk}\delta_{ij} = -2\nu_{sgs}\bar{S}_{ij} \quad (6)$$

$$\phi_j = -\alpha_t \frac{\partial \bar{T}}{\partial x_j} \quad (7)$$

Where, ν_{sgs} is the subgrid scale viscosity, α_t is the subgrid scale diffusivity, $\bar{S}_{ij}$ is the strain tensor rate defined as:

$$\bar{S}_{ij} = \frac{1}{2}\left(\frac{\partial \bar{u}_i}{\partial x_j} + \frac{\partial \bar{u}_j}{\partial x_i}\right) \quad (8)$$

The subgrid scale viscosity ν_{sgs} is defined by:

$$\nu_{sgs} = (C_s\bar{\Delta})^2|\bar{S}|, \text{où} |\bar{S}| = \left(\sqrt{2\bar{S}_{ij}\bar{S}_{ij}}\right) \quad (9)$$

$\bar{\Delta}$is the filter scale considered as the cubic root of the volume of the finite volume cell and C_s is the Smagorinsky constant.

The value of the constant model in this study was 0.1. In the same way ν_{sgs}, the subgrid scale diffusivity, α_t, is defined as follows:

$$\alpha_t = \frac{1}{Pr_t}(C_s\bar{\Delta})^2|\bar{S}| \quad (10)$$

Where Pr_t = 0.6 is the the subgrid scale Prandtl number. The Smagorinsky model is widely used in body bluff simulations (see [8] and [9]). It has also used the modeling of unresolved flows in simulations of heat transfer problems, see reference [10].

2.2.3 Mesh of the computational domain

In order to solve the Navier-Stokes equations, FLUENT 6.3 software based on the finite volume approach. For this configuration, the mesh used is structured quadrilateral multi-blocks was made using the software GAMBIT 2.4, presented in Fig.3. We get in this mesh 1185506 nodes or 1146000 cells hexahedral mesh well refined near the walls of the cylinder.

To the numerical calculation, the velocity-pressure coupling is achieved by Coupled algorithm.

The interpolation of the pressure is carried out by the interpolation scheme "body force weighted" and the terms of the transport equations is carried out by the interpolation scheme "Bounded Central Differencing" with relaxation factors in explicit form. The equation of energy is discretized by the interpolation scheme "Second Order Upwind".

All results, including the spectra (Fig.11) indicate that the resolution obtained is sufficient.

The time steps were such that the maximum number CFL was 0.83 and the Strouhal number St= 0.2. In this case we can calculate the frequency control of the convergence by the relation $f = (St.U_\infty)/D$ which must be equal to 2.7. Therefore, the flow time calculate is 8.88s with a time step Δt = 0.0148s.

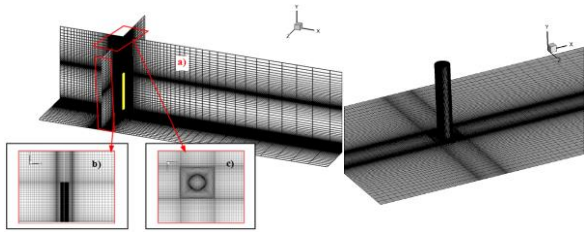

Fig.3: Non-regular mesh by block of the computational domain is 1146000 cells.

3 Validation of the results

The comparison of the results of the numerical simulation with those of the experiment of G. P. Salvador et al. [2], is shown in Fig.4.

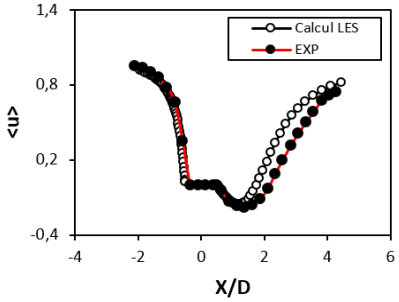

Fig.4: Distribution of mean longitudinal velocities <u> in the median plane (z = 0) at y/h= 0.6.

The average longitudinal velocity profile flow <u> in the median plane along the line y/h=0.6 obtained by LES gives a good agreement with the experimental velocity profile.

This comparison gives a validation of the numerical model LES used. So; the following calculations will be based on the chosen numerical model.

4 Results and discussion

In this section, we will analyze the qualitative and quantitative results interesting obtained from the numerical simulation, including the instantaneous and average velocity curves, the mean Nusselt number curves, the contours of the Q criterion and the turbulence statistics of the first and the second order.

4.1 The Dynamic analysis

4.1.1 Comparison of the velocity profiles

In the present study, we compare the mean and fluctuating longitudinal, lateral and vertical velocity profiles obtained by LES with those experimentally measured [2] (that its worked was carried out in the case of adiabatic flow where the absence of the thermal effect) along the longitudinal and vertical as well as transversal lines where the flow regime is supercritical with a number Reynolds $Re_D=2.2x10^4$ and for a density of heat flux imposed on the wall on the surface cylinder $\phi=600$ W/m^2.

Fig.5, shows the profiles of the longitudinal and vertical mean velocities u and v along the line's y/h=0.2 and 0.6, respectively, in the median plane. The mean longitudinal profiles <u> indicates a clear deceleration upstream of the cylinder, then they are zero at the passage of the cylinder and then they continue to decrease downstream thereof to the boundary of the recirculation zone. At the exit of this zone, the velocity profiles return to take the positive values in the wake zone. Whereas, for the vertical profiles <v>, at the upstream of cylinder they are zero, which translates the flow is purely developed along the axis ox, then they are zero during the passage of the cylinder, then downstream of it, they take a negative value.

These profiles are marked a maximum value at an abscissa x/D=2 in all cases whether experimental or simulation by LES. The upstream of cylinder, all profiles are given a good agreement with the experimental of [1], while downstream of it, they differ slightly from these, exclusively the longitudinal velocity profile at height y/h=0.6, which gave a better comparison. These different are marked in the zone behind the cylinder (in the wake zone).

Fig.6, shows the fluctuating velocities profiles of longitudinal and vertical, u and v, in the median plane along line y/h=0.2 and 0.6, respectively. It can be seen that the LES calculation is not badly compared with the experimental at the height y/h=0.6, whereas at y/h=0.2, there was some difference especially in the margin of y/h=0.9 to 2.2. For the maximum turbulence rate, was marked at x/D=0.25 in the all calculations whether by experience or by LES.

Fig.7, shows the evolutions of the averages and fluctuations longitudinal and vertical velocities profiles in the median plane (Z = 0) along the line x/D=1.We find that the profiles of the average velocities obtained by LES give an agreement with the experimental of [1].Whereas, the velocity fluctuation profiles obtained by LES are compared well with the experience of [1]. In the near wall the longitudinal and vertical velocity fluctuations are given rates of 25% and 10%, respectively.

Fig.8, shows the evolutions of the averages and fluctuating longitudinal and lateral velocity profiles along the lateral line at x/D=1.5 from the center and downstream of the cylinder in a height y/h=0.6. We observe that the velocity profiles obtained by LES whether longitudinal or lateral are similar with those experimental results.

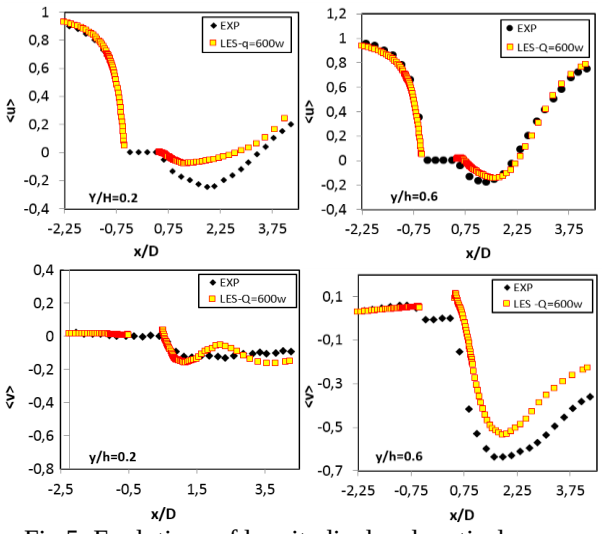

Fig.5: Evolutions of longitudinal and vertical averages velocities in the median plane at heights y/h=0.2 and 0.6.

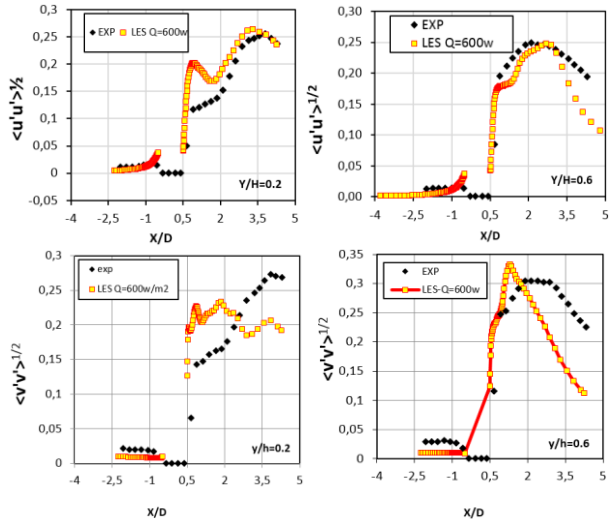

Fig.6: Evolutions of fluctuating velocities profiles of longitudinal and vertical in the median plane at heights y/h=0.2 and 0.6.

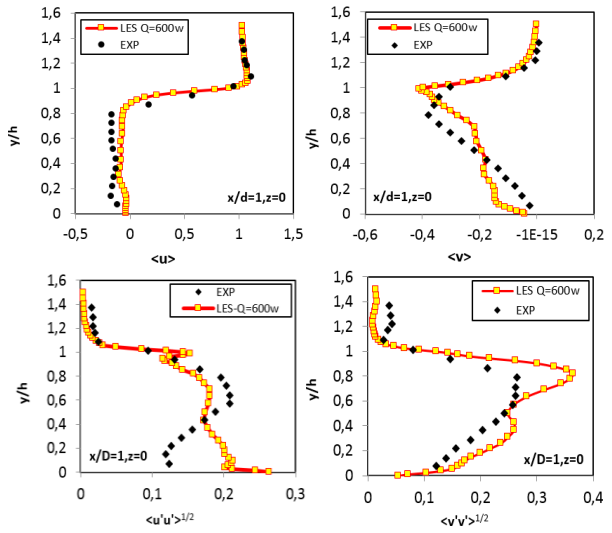

Fig.7: Evolutions of the averages and fluctuating longitudinal and vertical velocities along the line x/D=1 in the median downstream of the cylinder.

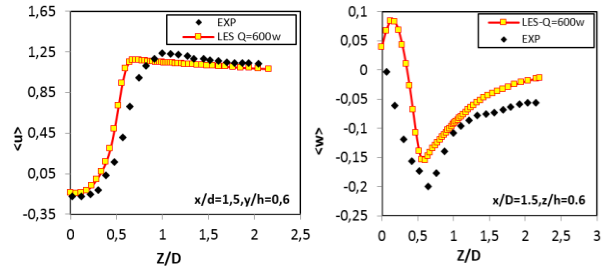

Fig.8: Evolutions of the averages and fluctuating profiles of the longitudinal and lateral velocities along the lateral line at x/D=1.5 from the center and downstream of the cylinder and in a height y/h=0.6.

4.1.2 Pressure coefficient profiles

The pressure coefficients obtained during our simulations are compared to the theoretical function, see the Fig.9. These coefficients are given for a perfect flow to vary according to the function $C_p=1-4\sin^2\theta$.

In order to analyze the obtained results, the theory indicate that the detachment zone is in the range ($60° \theta<120°$). At the leading edge of the cylinder we find values of C_p equal 0.6, which are corresponding to the same gaits, see the fig.9. They translate the points of stagnation (point of stops), where the pressure is maximum which is signified the zero velocity (the concordance of the Bernoulli equation).

In this figure the pressure coefficients plot for two heights y/h=0.5 and 0.8. We an increase of the absolute values of the pressure coefficient up to the maximum values $C_{Pmax}=1.78$ and 1.99 at y/h=0.2 and 0.6, respectively, corresponding the value of $\theta=77.1°$, and then they are constant in the remaining margin.

The angle of detachment which results in the point of separation is of order of $\theta_S=102°$, it is a value belongs in the zone of separation ($60°<\theta_S<120°$). So, the LES turbulence model gives a very good agreement for these margins of θ. These offsets of the average pressure coefficients are directly related to the type of boundary conditions imposed.

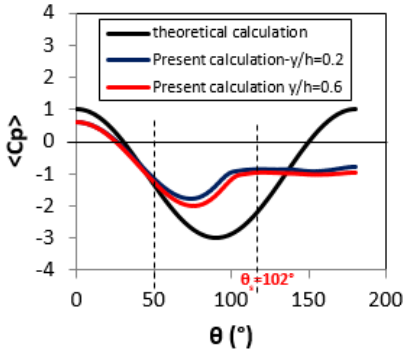

Fig.9: Evolutions of the theoretical pressure coefficient profiles for a perfect flow vary by the function Cp = 1-4sin2θ and our result at ϕ= 600W/m^2 at a height y/h= 0.5.

4.1.3 Visualization of mean and fluctuating fields

4.1.3.1 In the longitudinal center plane

Fig. 10 and 11, show the streamlines followed by the average longitudinal velocity fields dimensioned by the upstream velocity of fluid, streamwise and spanwise velocities fluctuations fields which are plotted in the longitudinal center plane of the cylinder (z=0). It is found that the mean streamwise velocity <u> is important above the shear layer, which is translated in an acceleration of the flow, and a recirculation zone behind the cylinder has appeared and is limited by a separation line. While,

streamwise and spanwise velocities fluctuations are important in the recirculation zone of the flow, behind the cylinder and close to the middle thereof, respectively. These fields flow are marked with a maximum value near to 0.3 m/s which has been found experimentally by [2].

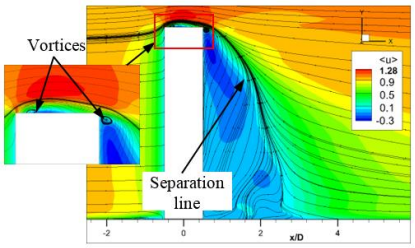

Fig.10: Mean streamlines and streamwise velocity fields on the mid-transverse plane (z/D = 0).

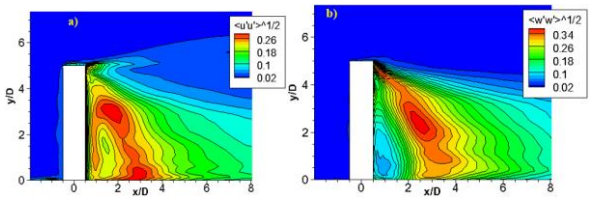

Fig.11: Root mean square of the streamwise (u') and spanwise (w') fluctuations on the mid-transverse plane (z/D = 0).

4.1.3.2 In horizontal planes

The fall of the flow passing through a free end cylinder is now studied in more detail by an analysis thereof behind the cylinder and especially in horizontal planes around the base plate and at different heights at y/h= 0.6 and 0.8.

Fig. 12-a to 12-h provide iso-contours of <u>, $\langle u'u' \rangle^{1/2}$, $\langle w'w' \rangle^{1/2}$, <u'w'>, mean and fluctuating streamwise and spanwise velocities, plotted in two parallel planes at y/h=0.6 and y/h=0.8.

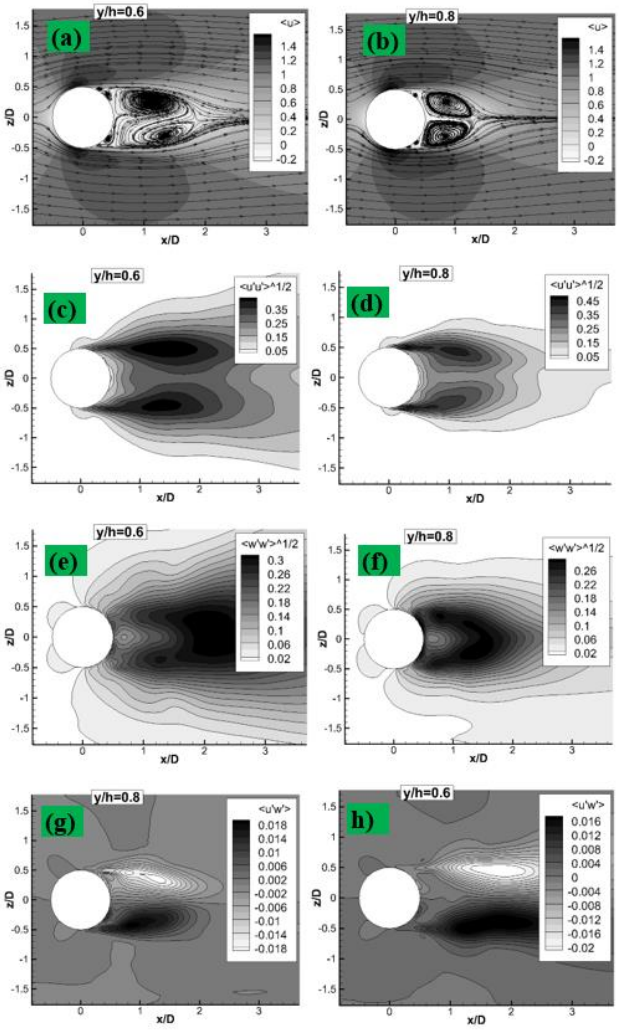

Fig.12: Mean-streamlines and iso-contours of the mean and fluctuating streamwise and spanwise velocities, plotted in two parallel planes at y/h=0.6 and y/h=0.8 in instant a time ts=4.44s.

At y/h=0.6, in the fig.12 the streamlines show the same behavior of a flow around a circular cylinder, that is to say there are more elongated and unsymmetrical separation bubbles and the stagnation point is located at x/D=2. Whereas, at y/h=0.8 near the free end of the cylinder, we noticed a shorter and symmetrical separation bubbles and the points of separation and stagnation which are located at θ_S=72° and at x/D=1.5, respectively.

However, when we move downward, we observe a certain elongation of the recirculation zone and other secondary bubble appeared and the symmetry was absent. This remark is translated by backing of marginal vortices created by the trailing edge above the cylinder, then inclined and directed towards the ground due to the load weight. These results are similar to each other in comparison with those of [2] and the numerical calculation of Lecocq Y. [3].

4.1.4 Vortices structures of the flow

In this work, the numerical simulations of flow around a cylinder are carried out by the LES approach in a subcritical regime at Reynolds number $Re_D=2.2x10^4$ in the range $300 \leq Re_D \leq 2 \cdot 10^5$. The flow passing through a free end cylinder causing a pressure difference between the base and the edge thereof induced by a flow deflection and the creation of marginal vortices, also called secondary flow. These behaviors may be to cause:

- An expansion of the area downstream of the cylinder translated by formations vortex and the extent of the area near wake following the intensity of this deflection (when the Strouhal number decreases).
- A non-existent vortex shedding for low aspect ratio values; the figure 2.16 shows that the secondary flow then becomes the main flow.

The criteria presented above pose a major difficulty for the configuration study presenting the situations of the flow around a free end cylinder. We present in the rest of this paragraph criteria based on the tensor components of velocity gradient $\frac{\partial u_i}{\partial x_j}$.

Criteria for the function Q

The definition of a vortex given by Hunt et al. (1988) calling the second invariant Q of $\overrightarrow{\text{gradu}}$. Q is then defined: $Q = \frac{1}{2}\left(\Omega_{ij}\Omega_{ij} - S_{ij}S_{ij}\right)$.

Or; *Sij* and *Ωij* represents the symmetrical and asymmetrical portions of the velocity gradient tensor. So: $S_{ij} = \frac{1}{2}\left(\frac{\partial u_i}{\partial x_j} + \frac{\partial u_j}{\partial x_i}\right)$ *and* $\Omega_{ij} = \frac{1}{2}\left(\frac{\partial u_i}{\partial x_j} - \frac{\partial u_j}{\partial x_i}\right)$.

Thus, physically, the regions where Q is negative represent the regions where the vorticity is greater than the deformation. This criterion will therefore be more efficient than the norm of vorticity alone in the near-wall zones.

The criterion based on the norm of the vorticity offers the very parasitized views by the strong shear regions. Following observations that were found or represented by Kawamura et al. [1], P. G. Salvador et al. [2], Y. Lecocq [3] and others, we privileged the use of the criterion Q for the visualization of coherent structures in our simulations.

Basing on the instantaneous characteristics of the solution obtained by the LES calculation. An overview of the flow is shown in fig.13. We present in the first place the iso-surface of the criterion-Q, such that Q = 20. It is found that the overall behavior of the flow is clear.

Fig.13, shows the presence of a horseshoe tourbillon, noted TFC1, marginal vortices, TM, Trailing Vortices, denoted TV 1 and 2, Von Karman vortices (VKV), Kelvin-Helmholtz vortices (KHV) and Hairpin vortices (TEC).

We observe a sudden deflection fluid just after the cylinder. Marginal vortices, TM, are driven to y/h<1 and probably intersect with Von Karman vortices (VKV). We can also see the nascent horseshoe vortex upstream of the cylinder and then the separation of its legs when the fluid passes the cylinder. These structures will be seen in more detail in Figs. 15 on sectional planes.

Still in FIG. 13, the Kelvin-Helmholtz vortices (KHV) originating from the detachment of the lateral boundary layers are observed. The axis of these vortices is almost rectilinear on the portion y/h∈ (1/4, 3/4) with respect to the axis of the cylinder in the plane (xoz) and is inclined outside. The curvature of these vortices is certainly related to the increase of the velocity when y/H>3/4 and not to the slope of the velocity profile imposed at the entrance of the domain of computation. End eddies greatly influence the wake of flow for this aspect ratio.

The temporal evolution of the instantaneous flow is shown in FIG. 10 in the constant margin non-dimensional time $\Delta t^* = (\Delta t.u_\infty)/D=10$. This figure represents the whole of the three-dimensional (3D) flow, in particular, the vortices formed around the side and behind the cylinder visualized using the iso-surfaces of the of the wheel invariant<Q> = 20 to left and <Q> = 50 on the right. These vortex structures, globally, give the same images as observed in Figure 1 plotted by Boizumault et al. [1].

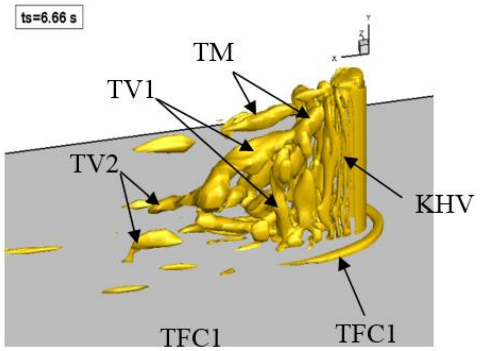

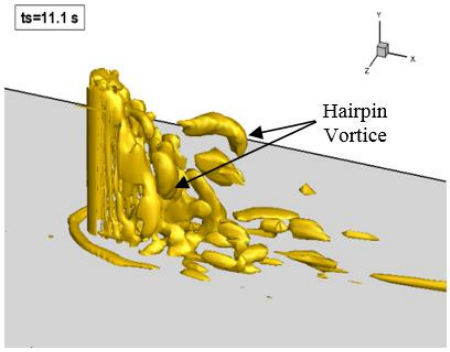

Figure 13. Instantaneous values of the invariant Q: inclined view for Q = 20 s^{-2}, at time step $\Delta t^*=(\Delta t.u_\infty)/D=10$.

Instantaneous flow visualization

In the transverse planes

As can be seen in Figures 15 (a), in the plane x/D=0.3, reveals the presence of two pairs of vortices: the first, identified as the marginal vortices TM is located in z/H~0.9 as one enters the wake and the second pair in the near end of top of the cylinder in z/H~1. This second pair, inside the first and rotating in the opposite direction of each end vortex is called by these authors Tornado-like vortices, which will be called later TLV. Kelvin-Helmholtz vortices (KHV) are also observed in the ¼ diameter part of the cylinder towards the wake zone.

Plan x/D=1 and 1.5, Figure 15 (c), (d), (e) and (f) reveals two vortices called in the Trailing Vortices literature in English and subsequently in this TV. There can be no question of the tourbillon horseshoe either because this structure is much too small (compared to those mentioned) and secondly it is confined to the region of near wall whose trace is visible in the lower corners left and right of each plane (TFC).

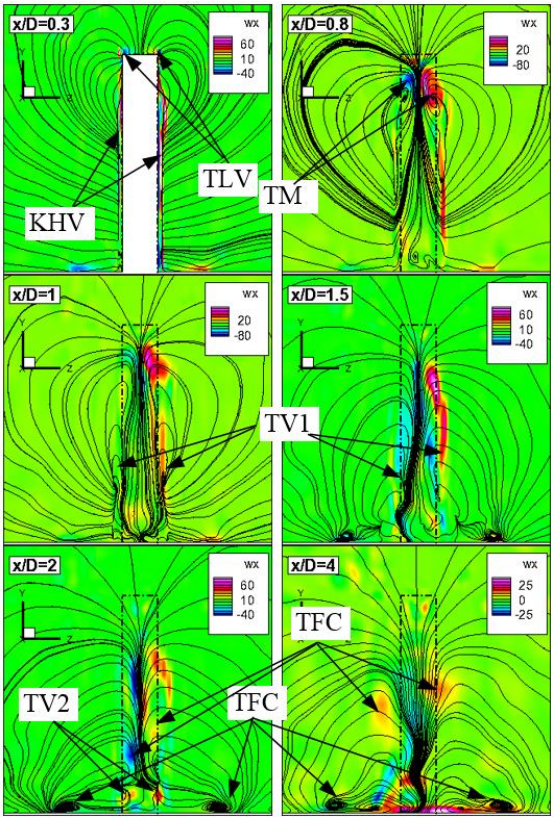

Fig.15: Average-time streamlines and contours of the instantaneous longitudinal vorticity ($\tilde{\omega}_x$) at x/D=0.3, 0.8, 1, 1.5, 2 and 4 at moment time t_s = 4.44s.

Power spectral analysis for CL

It is important to say here that for Re = $2.2x10^4$, the flow regime is subcritical, it is verified the condition $300 \leq Re \leq 2.10^5$. The analysis of the power spectrum of the lift coefficient in Figure 16 clearly shows the existence of a broad and continuous spectrum, the characteristics of a wake regime is stable. This analysis clearly indicates the presence of interaction frequency of the cylinder. The highest peak on this figure corresponding the frequency to leave of the primary vortex of Von Kàrmàn, which corresponds to a Strouhal number = 0.122.

Flow on the cylinder walls

The streamlines on the cylinder surface are shown in fig.12. The flow behaviour computed by LES is well captured. On the cylinder top (Figure 12-e), two rattachment and separation (singular points) points located at x/D~0.1135 et 0.334, respectively, and two small bubbles (noted Foyer) marked at x/D~0.062 and z/D~0.356 in the plane (xoz) almost symmetrical about the median plane at z = 0 are observed. On the vertical walls of the front view (figure 12-c) shows the separation line directed slightly upwards going into the walls of the cylinder. Near the cylinder bord, the stagnation line

splits into a current line fan due to the end effect. The side view (fig.12-b), shows the separation line at a fairly constant angle of 84.3° relative the axis ox. This line is therefore largely vertical and in the upper end is slightly curved towards the median plane (z = 0). In the back and below ends region, there is a vortex and a singular points node-like of separation, there the motion is directed upwards, downwards and sideways.

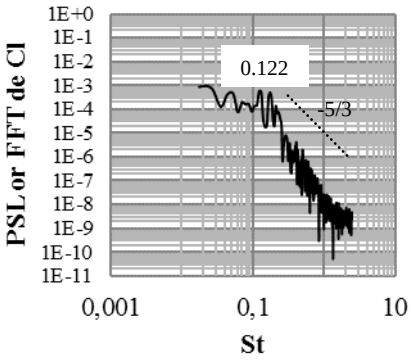

Fig.16: Power spectral density function of lift on the finite-length cylinder. The straight dotted line has a slope of -5/3 in the logarithmic curve.

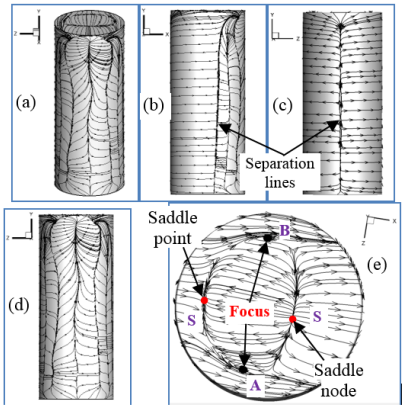

Figure 17. Streamlines of flow on the surfaces cylinder: a) Rear face, b) Side face, c) Front face, d) Above face and near the ground (e) for H/D=5.

Thermal analysis

Température fields

In heat transfer by forced convection, the thermal field is combined by the dynamic field. Thus, the number of Nusselt can be calculated according to the characteristics of the dynamic regime considered. It is possible to find global relations involving the Reynolds number with the Prandtl number according to the following correlation:

$$\langle \overline{Nu} \rangle = cRe^{m}Pr^{n} \qquad (11)$$

where $\langle \overline{Nu} \rangle$ represents the mean of the Nusselt number. One can also find local correlations i.e. involving for example the angle reflecting the thickening of the mechanical boundary layer (sum of the dynamic and thermal limit layers), according to Eckert [15] the number of Nusselt in this case is written:

$$\frac{\langle \overline{Nu} \rangle}{\sqrt{Re}} = 0.57Pr^{0.7}\sqrt{3.6314 - 2.1709\left(\frac{\theta}{2}\right)^{2} - 1.5144\left(\frac{\theta}{2}\right)^{4}} \qquad (12)$$

Finally, it is possible to characterize the heat transfer over the entire circumference of the cylinder and thus take into account the separation of the boundary layer which is followed by the appearance of a medium flow recirculation zone which intervene. on its surface.

Sanitjai & Goldstein [16] distinguish three zones in which different correlations can be applied.

- The first one is the one where the Nusselt number is monotonically decreasing as a function of θ due to the thickening of the boundary layer until its detachment, $\langle Nu_{0°-85°} \rangle$, equation (13). At this position the observed minimum is an overall minimum. According to Bailer et al. [17] who performed numerical simulations at Re = 200 and Re = 2000, it seems that the heat transfer in this first zone is independent of time.

$$\langle Nu_{0°-85°} \rangle = 0.945Re^{0.5}Pr^{0.35} \qquad (13)$$

- The second zone is between the detachment and the second minimum, local this time, $\langle Nu_{85°-135°} \rangle$ equation (14). There is an increase in heat transfer that is proportional to the Reynolds number.

$$\langle Nu_{85°-135°} \rangle = 0.072Re^{0.7}Pr^{0.41} \qquad (14)$$

- In the third zone, there is an increase in the Nusselt number due to vortex shedding, $\langle Nu_{135°-180°} \rangle$, equation (15). The last two zones are dependent on the Reynolds number but also on the incident turbulence.

$$\langle Nu_{135°-180°} \rangle = 0.037Re^{0.8}Pr^{0.42} \qquad (15)$$

On the contrary, tangentially to the wall, the speed of the water increases along the front face from the point of attack, then decreases along the rear face. When the velocity gradient is zero, the boundary layer separates from the wall and convective heat exchange reaches a minimum. The

separate flow area at the rear of the cylinder appears to be turbulent. These general flow behaviors are well observed in the velocity profiles indicated above.

Nusselt Numbers profiles

The effect of the heating of a cylinder on the water flow is less important, due of the difference between the reference temperature flow and the average surface temperature calculated from the Neumann condition. Y. Lecocq [3] has shown that there is a major effect of the heating on the overall structure of the flow behind the cylinder. For this reason, the Nusselt number can be presented in FIG. 13 for two height levels at y/h=0.2,0.5, 0.6 and 1 as a function of the rotation angle θ of the cylinder.

It can be seen that, for y/h=1, the evolutions of the profiles are based on the typical image of the flow around a circular cylinder, while for the others nearly they conform between (-112° and 100°). In addition, when moving downwards, the angles are taken the positive values of (100° to 180°) and from (-112° to -180°) the evolutions are superimposed on each other with lower Nusselt values.

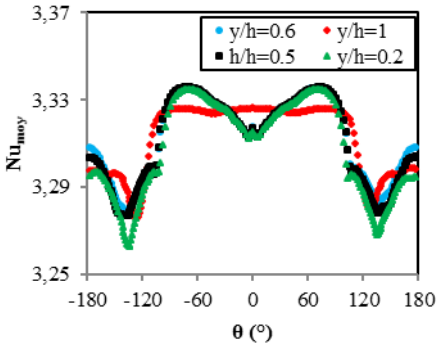

Figure 18. Evolutions of the average Nusselt number profiles at different heights y/h=0.2,0.5, 0.6 and 1 as a function of the rotation angle θ of the cylinder.

Instantaneous average and fluctuating temperature fields

Figures 19 and 20 show the fields of the instantaneous average and fluctuating temperatures in different cross-sectional planes, x/D=0.3, 0.8, 1, 1.5, 2 and 4 and for a density of the heat flux imposed on the cylinder of 600 W/m^2. It can be seen in both figures and for all transverse planes that the two types of temperature are marked with maximum values near the ground. When moving towards the rear of the cylinder, it is observed that the heat is diffused well towards the ground in an almost symmetrical manner.

These observations due to the strong deflection of the water down which fell not far from the cylinder in the wake. This fluid is also responsible for transporting heat from the cylinder to the wake zone, where heat transfer can be defined by forced convection.

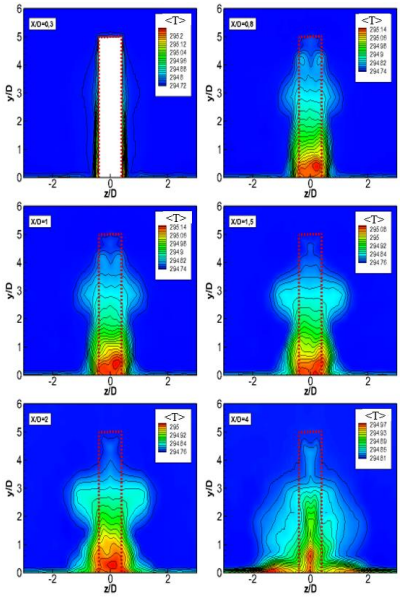

Figure 19: Contours of instantaneous average température <T> in y-z planes at 6 consecutive streamwise locations: x/D=0.3, 0.8, 1, 1.5, 2 and 4 in instant a time ts = 11.84s.

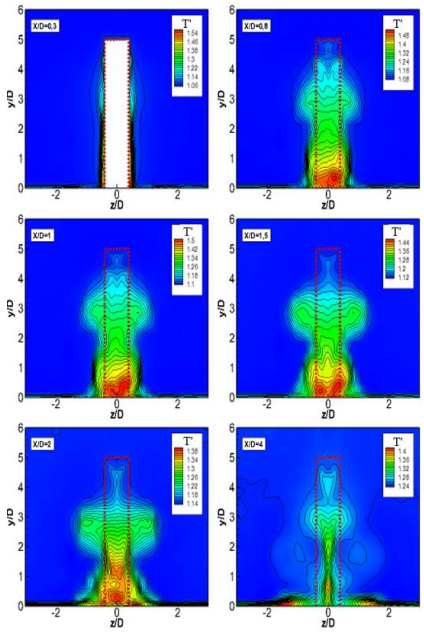

Fig.20: Contours of instantaneous fluctuating température T' in y-z planes at 6 consecutive streamwise locations: x/D=0.3, 0.8, 1, 1.5, 2 and 4 in instant a time ts = 11.84s.

To give another explanation for the convective heat transfer, we will present the fields of the mean and fluctuating surface temperatures of the cylinder in Figure 16. It is found that the average and

fluctuating temperatures have marked maximum values close to 295.25 K and 1.6 K, respectively near ground.

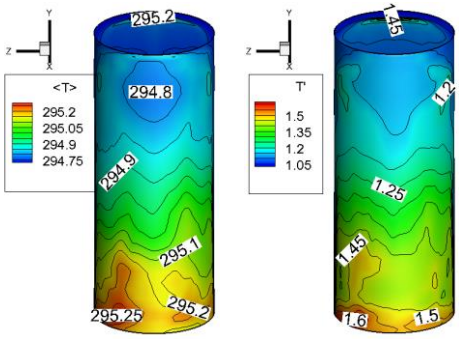

Fig.21: Evolutions of the average and fluctuating surface temperatures fields of the cylinder.

4 Conclusion

Large Scale Simulation (LES) has been used successfully to study the viscous incompressible flow around a circular cylinder thermally heated on its surface by an imposed heat flux density ϕ = 600W/m^2. It is mounted vertically on an adiabatic flat wall and with an aspect ratio AR=H/D=5.

The obtained results by LES have made it possible to analysed and present the necessary fields flow, such as, mean and fluctuating velocities fields in the three directions, as well as the instantaneous fields which are presented by iso-surfaces of the criterion Q. Finally, the average Nusselt number presenting for different heights. From this work it can be seen that forced convection heat exchange is well carried out. Generally, the results obtained are consistent with those found experimentally and numerically.

References:

[1] Kawamura, T., Hiwada M., Hibino T, Mabuchi I., and Kamuda M, Flow around a finite circular cylinder in a flat plate. (1984) *Bull. JSME*, 27(232) :2412–2151.

[2] P. Salvador G., Thorsten S.,Jochen F., Michael K., Wolfgang R.et al, Large Eddy Simulations and Experiments of Flow around Finite-Height Cylinders, (2009) *Flow Turbulence Combust*, 84:239–275, 21 August.

[3] Lecocq Y., contribution à l'analyse et à la modélisation des écoulements turbulents en régime de convection mixte –application à l'entreposage des d´déchets radioactifs, (2008) *thèse de Doctorat de l'université de Poitiers*.

[4] Norberg C., An experimental investigation of the flow around a circular cylinder: influence of aspect ratio, (1994) *J . Fluid Mech*., nol. 258, p p . 287-316.

[5] Persillon H, Braza M., Physical analysis of the transition to turbulence in the wake of a circular cylinder by three-dimensional Navier-Stokes simulation, (1998) *J. Fluid Mech*.vol. 365, pp.23-88.

[6] Germano, M., Piomelli, U., Moin, P., Cabot, W.H., A dynamic subgrid-scale eddy viscosity model, (1991) *Phys. Fluids*3,1760-1765.

[7] Lilly D.K., A proposed modification of the Germano subgrid-scale closure method, (1992) *Phys. Fluids* 4, 633–635.

[8] Hemida H., Large-Eddy Simulation of the Flow around Simplified High-Speed Trains under Side Wind Conditions, (2006) *thesis of Lic. Of Engng, Division of Fluid Dynamics*, Universit de Chalmers of Technology, Göteborg, Sweden.

[9] Krajnović S., Davidson L., Flow around a Simplified car, Part (1): Large-Eddy Simulation", (2005) *Journal of Fluid Engineering*, Vol. 127, pp. 907-918.

[10] Barhaghi D., Davidson L., Karlsson R., Large Eddy Simulation of Natural Convection Boundary Layer on a Vertical Cylinder, Selected paper, (2006) *International Journal of Heat and Fluid Flow*, to appear.

[11] T. Rödiger, H. Knauss, U. Gaisbauer, E. Krämer, Pressure and Heat Flux Measurements on the Surface of a Low-Aspect-Ratio Circular Cylinder Mounted on a Ground Plate, 96 New Results in Numerical and Experimental Fluid Mechanics VI: Contributions to the 15th STAB/DGLR Symposium Darmstadt, Germany, 121-126. 2006.

[12] Kappler, M.: Experimentelle Untersuchung der Umströmung von Kreiszylindern mit ausgeprägt dreidimensionalen Effekten. Ph.D. thesis, University of Karlsruhe. http://digbib.ubka.uni-karlsruhe. De /volltexte/12232002 (2002).

[13] Donnert, G.D., Kappler, M., Rodi, W.: Measurement of tracer concentration in the flow of finite-height cylinders. Jornal of Turbulence. **8**(33), 1–18 (2007).

[14] Etzold, F., Fiedler, H. The near-wake structure of a cantilevered cylinder in a cross flow. Zeitschrift für Flugwissenschaften 24, S. 77-82 1976.

[15] E. R. G. Eckert. Die berechnung des w¨arme¨uberganges in der laminaren renzschicht umstr¨omter k¨orper. VDI-Foshungsheft 416, 1942.

[16] S. Sanitjai and R. J. Goldstein. Forced convection heat transfer from circular cylinder in crossflow to air and liquids. Int. J. of Heat and Mass transfer, 47 :4795–4805, 2004.

[17] F. Bailer, P. Tochon, J.-M. Grillot, and P. Mercier. Simulation numérique de l'écoulement et transfert de chaleur autour d'un cylindre. In Elsevier, editor, Revue Générale de Thermique, volume 36, pages 744–754. 1997